Hindawi
Geofluids
Volume 2020, Article ID 8543687, 12 pages
https://doi.org/10.1155/2020/8543687

Research Article

Experimental Study on Seepage Characteristics of Jurassic Weakly Cemented Sandstone under Water-Rock Interaction

Qin Liu,[1] **Yajun Sun**,[2] **and Jian Li**[3]

[1]*College of Mining Engineering, Taiyuan University of Technology, Taiyuan 030024, China*
[2]*School of Resources and Geosciences, China University of Mining and Technology, Xuzhou 221116, China*
[3]*Shanxi Institute of Geology and Mineral Resources, Taiyuan 030006, China*

Correspondence should be addressed to Qin Liu; lq_cumt@live.cn

Received 6 August 2019; Accepted 1 May 2020; Published 21 May 2020

Academic Editor: Shengnan Nancy Chen

As unconventional water-bearing rocks, the hydraulic conductivity of weakly cemented sandstones can increase by several orders of magnitude during drainages or pumping tests, posing great challenges to water prevention and control of coal mines in northwestern China. In this study, seepage experiments on Jurassic weakly cemented sandstones were performed and the hydraulic conductivity during the seepage process was analyzed. Combined with laboratory test and theoretical analysis methods, the relation between the permeability and micropore structures was studied, and the permeability evolution mechanism of the weakly cemented sandstones was eventually clarified. According to the experimental results, the seepage process can be divided into the saturated seepage stage, the stable seepage stage, and the seepage mutation stage. The hydraulic conductivity increases as the porosity and the mercury extrusion rate increase, but there is no obvious correlation between them that can be identified. In contrast, there is a linear positive correlation between the hydraulic conductivity and the average pore-throat radius. The variation trend of the pore-throat ratio can be used as the main reference indicator for judging whether the seepage mutation occurs in weakly cemented sandstone. Based on the correlation analysis of micropore structures and the hydraulic conductivity, a seepage model of straight capillary was constructed and the theoretical permeability equations of stable seepage stage and seepage mutation stage were proposed. It is concluded that the specific permeability of weakly cemented sandstones is directly proportional to porosity and the square of the average pore-throat radius. A theoretical equation to calculate the specific permeability during the latter two stages was also presented in this paper. Theoretical calculation results are roughly consistent with actual values obtained in the experiments.

1. Introduction

Jurassic and Cretaceous weakly cemented strata are widespread in western China due to the special diagenetic environment [1, 2]. The weakly cemented strata are dominated by sandstones, which are characterized by poor cementation, susceptibility to weathering, high porosity, and low strength [3]. They are significantly different from normal sandstones and soft rocks in terms of cementation, mechanical, and hydraulic properties. Due to these special sandstones, huge and unstable water inrush occurs in some coal mines of Xinjiang province, which can easily trigger a disaster. As pumping tests of Dananhu No. 5 coal mine carried on in the Hami mining area of Xinjiang, the hydraulic conductivity of weakly cemented sandstones continued to increase [4]. The hydraulic conductivity increased gradually from 0.18 m/d of initial coalfield exploration data to 4.33 m/d of the later stage of pumping experiment. During a large-scale drainage project in Yili No. 1 coal mine, it took initially three months for the water level of observation wells about 200 m away from the evacuation center began to fall. This time interval decreased to 10 minutes at last. At the same time, the permeability of aquifer has been increased and the connectivity of pores and fractures improved. The increase of hydraulic conductivity of aquifer by several orders of magnitude brings a great challenge for water control and drainage in coal mines. The loss of water resources has a great impact on the ecological environment. It is necessary to conduct a

comprehensive study on the hydraulic properties and the evolution mechanism of the permeability of weakly cemented sandstones to address these issues.

Krishnan et al. [5] managed to prepare samples of weakly cemented sandstones firstly and analyzed microscopic features of broken rocks. Wang et al. [2] observed intact sandstones from Jurassic weakly cemented strata using a scanning electronic microscope (SEM), and various tests were further performed to determine the quantitative relationships among mineral concentrations and physical and mechanical parameters. Zhang et al. [6] reported the evolution mechanism of the porosity as clay minerals changed in weakly cemented sandstones. You et al. [7] discovered that the larger confining pressure would result in the plastic deformation among the grains in weakly cemented sandstones, as well as an irreversible decrease of specific permeability. An effective method to estimate macropermeability coefficients using images of SEM was proposed by Yu et al. [8] and Li et al. [9]. Wang et al. [2] estimated the specific permeability using regression analysis based on geometric parameters including pore areas, perimeter and fractal dimension. Bloch and Helmold [10] developed a method to estimate specific permeability by particle-size distribution. Lala [11] suggested to estimate the absolute permeability with pressure data of mercury injection capillary experiments. As core samples of weakly cemented sandstones are very difficult to make due to their low strength and weak adhesion, researches on water-rock interaction have been rather scarce. When it comes to permeability models, Herron [12] reported a linear correlation between the logarithm of specific permeability and porosity according to his study on oil reservoirs of single-porosity sandstones. Kozeny [13] and Carman [14] established a relation among the permeability, porosity, and surface area for homogeneous medium based on the capillary theory, namely, Kozeny-Carman formula. Timur [15, 16] put forward a formula of specific permeability, porosity, and irreducible water saturation, while Krumbein and Monk [17] presented a relation among the specific permeability, the average grain size, and sorting.

Researchers across the world have conducted extensive studies on the permeability models and established various formulas for the specific permeability. Most of these studies focus on hard or compact rocks, which means that studies on seepage characteristics of weakly cemented sandstones with high porosity and changeable permeability are scarce. The mechanism for the increase of the specific permeability by several orders of magnitude in weakly cemented sandstones remains unknown. In this study, we performed seepage experiments on intact core samples of Jurassic weakly cemented sandstones collected from Hami mining area. The change of their mineral composition and micropore structures was analyzed during the experiments. A seepage model was established to demonstrate the mechanism of permeability evolution of weakly cemented sandstones. In combination with theoretical analysis, we proposed an equation for the specific permeability of weakly cemented sandstones.

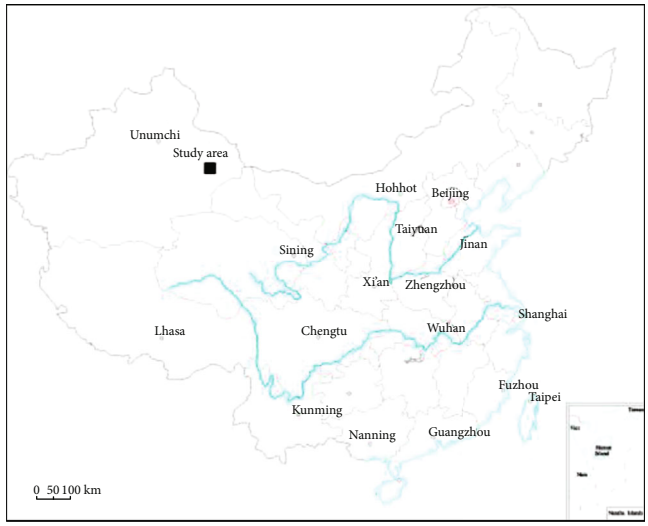

Figure 1: The locality of the study area.

Table 1: Variation of hydrogeological parameters of weakly cemented sandstones.

Stage	K (m/d)	q (1/s·m)
Detailed survey	$1.64 * 10^{-4}$	0.0002
Exploration	$3.06 * 10^{-1}$	0.2370
Drainage	$5.06 * 10^{-1}$	0.3500
Pumping test	4.33	1.1800

2. Background of the Study Area

The III-1 aquifer of weakly cemented sandstones in Hami mining area is identified as Jurassic Xishanyao formation [18] (Figure 1). It is composed by siltstones, fine-grained sandstones, medium-grained sandstones, conglomerates, and sandy mudstones. The study area, located near the city of Hami in Xinjiang province, is generally an arid region. Yet when the rockshaft was drilled through the III-1 aquifer, the water yield of mine reached 113 m^3/h. After a long-term drainage through 22 draining holes on the ground, a total amount of 8.21 million m^3 water was drained away. The hydraulic conductivity of the aquifer reached 0.56 m/d, 1.6 times larger than that obtained from coalfield exploration. In comparison with the data obtained during the detailed survey stage, it increased by three orders of magnitude (Table 1). To ensure the security of the initial mining face, a twenty-day pumping test of large discharge, deep drawdown, and longtime delay was conducted. Eventually, the hydraulic conductivity of the aquifer increased again by an order of magnitude, reaching 4.33 m/d [4].

As the water flow of drainage surges, the hydraulic conductivity of the aquifer increases substantially accompanied by the transformation of pore structures. To ascertain the specific mechanism and pattern of the change of permeability, a specific indoor seepage experiment was designed and carried out.

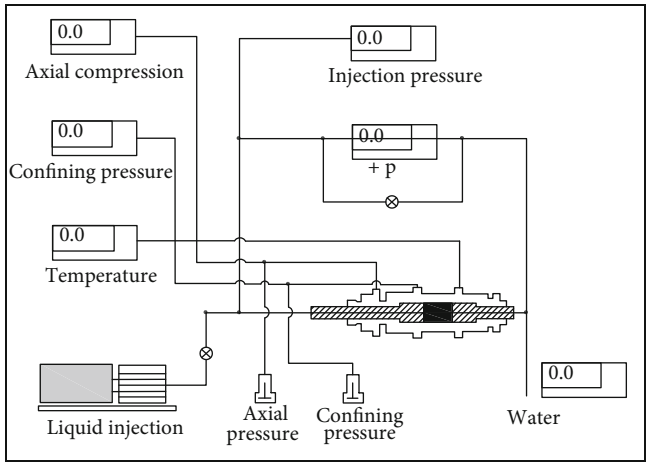

Figure 2: A schematic image of the seepage experimental system.

3. Materials and Methodology

3.1. Methodology. As shown in the technology roadmap (S1), steady seepage experiments and other analytical methods were used to investigate the evolution characteristics and mechanism of the permeability of weakly cemented sandstones.

(1) By a comparative study on micropore structures of the sandstones before and after the seepage experiments, the pattern of the transformation of micropore structures were investigated

(2) To clarify the evolution mechanism of micropore structures under water-rock interaction, the material in the aqueous solution produced by the seepage experiments was identified and measured their content through hydrochemical tests, X-ray diffraction (XRD), and scanning electronic microscope (SEM)

(3) Based on the evolution characteristics of the permeability during the seepage experiments, the coupling relationship between the microstructure parameters and specific permeability was established. The starting conditions and discrimination criteria of the seepage mutation under water-rock interaction should be further analyzed and revealed

(4) A seepage model and equations were proposed on the basis of Darcy's law and capillary theory. The permeability equation is fitted and matched with the experimental data of the seepage experiments to verify its accuracy and practicability

3.2. Experiment Equipment. Indoor seepage experiments appear as an efficient tool for understanding the permeability evolution characteristics of weakly cemented sandstones. Inspired by the latest research results and experimental equipment [19, 20], a set of instruments for seepage experiments under water-rock interaction of weakly cemented sandstones was improved and assembled (Figure 2). The experimental equipment consists of rock sample loading and permeation system, axial pressure loading system, confining pressure loading system, pressure sensor, temperature sensor, and automatic recording balance.

Figure 3: Images of the core samples.

3.3. Sample Material and Preparation. Weakly cemented sandstones in the study area consist of siltstones, fine-grained sandstones, medium-grained sandstones, and conglomerates. The rock samples were taken from the Jurassic Xishanyao formation of Dananhu mining area by drilling, with a buried depth of about 200 m. And the selected rock samples were complete without cracks. As medium-grained sandstones are more homogeneous than others, they are better objects for studying the microstructural features of weakly cemented sandstones. Sample preparation is also easier. Therefore, core samples of this study are made from medium-grained sandstones using a hole opener without using water. The hole opener has an interior diameter of 25 mm and an exterior diameter of 32 mm.

(1) As the samples are weakly cemented, fracture often occurs during the sample preparation, making it very difficult to obtain perfect standard core samples. As shown in Figure 3, twenty core samples with diameters larger than 24 mm and lengths exceeding 10 mm were picked out of fifty alternative samples

(2) As the remaining parts of the rock samples have not been deformed and destroyed (Figure 3), the analytical results of composition, structures, and hydraulic properties are highly consistent with those of core rock samples. This kind of rock should be the best object for reference. Mercury intrusion experiments and SEM analysis were conducted for the comparative study

(3) To make sure that the pressure on core samples are evenly distributed and structures of samples will not be damaged by pressure, both the top and bottom surfaces of core samples are polished using a buffing machine

(4) Special waterproof tapes were wounded on the core samples to prevent boundary seepage. Core samples are also in close contact with the device in this way

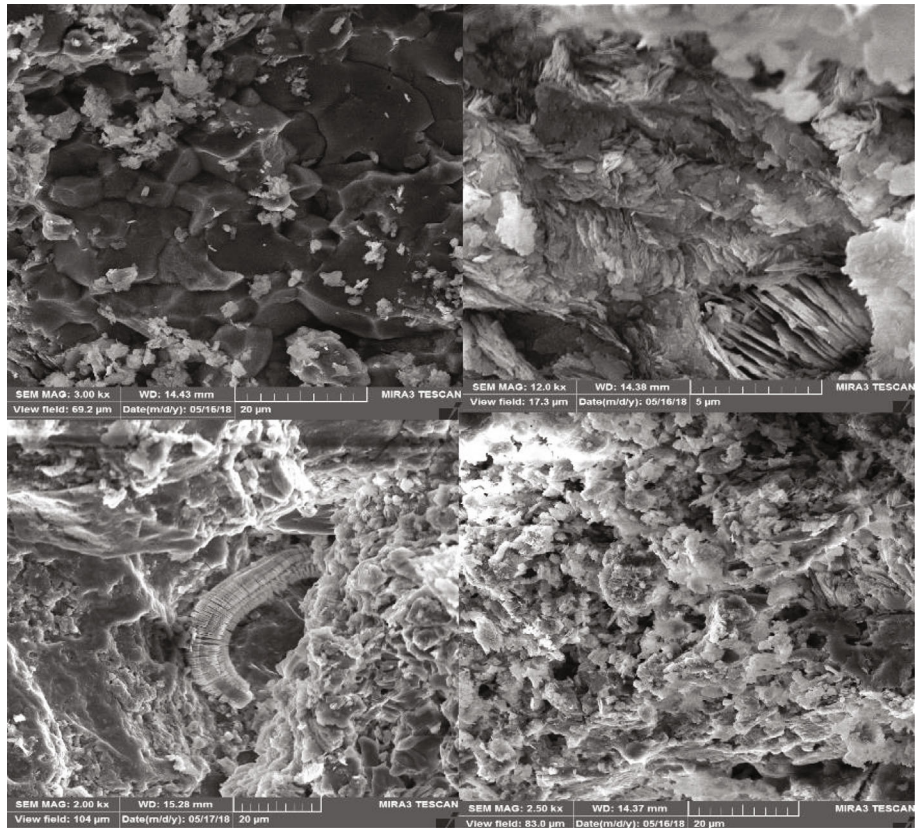

Figure 4: The framework of weakly cemented sandstones by SEM.

3.4. Parameter Preparation. According to the images of SEM (Figure 4), the samples from this seepage test are medium grain sandstones without any cracks, but different types of microcracks and voids in the disorderly distributed feldspar particles or quartz particles. The pores are naturally heterogeneously distributed in sandstones. Jacob Bell obtained the relationship between seepage velocity and hydraulic gradient through a large number of experiments. When the Reynolds coefficient (Re) is less than 10, the correlation curve is positive linear correlation, and the groundwater movement obeys Darcy's law [21]. The average grain diameter of weakly cemented sandstone is 200 μm, and the Reynolds coefficient is far less than 1. The seepage experiment in this study accords with Darcy's law. Real-time observation of the hydraulic conductivity k_i is achieved by calculations based on Darcy's law. The formula is as follows.

$$k_i = \frac{Q_i \cdot L}{A \cdot \Delta h \cdot t}. \quad (1)$$

In order to choose the proper confining pressure and axial pressure, preliminary seepage experiments were conducted on saturated weakly cemented sandstones (sample YP-24-1), applying different confining pressure and axial compression (1.5 MPa, 2.5 MPa, 3.5 MPa, 4.5 MPa, and 5.5 MPa). The injection water pressure was set at 0.45 MPa. The variation curve of hydraulic conductivity with time is presented based on Equation (1). As shown in Figure 5, large variations occur in hydraulic conductivity when the confining pressure is 1.5, 4.5, and 5.5 MPa. When the confining pressure is 2.5 and 3.5 MPa, variations of hydraulic conductivity are rather small. The average values of hydraulic conductivity are roughly the same (average = 0.00014 m/d). According to the results of preliminary seepage experiments, confining pressure and axial compression are set synchronously at 2.5 MPa with an injection pressure of 0.45 MPa.

4. Experimental Process and Results

4.1. Experimental Process. Seepage experiments were conducted on fifty samples under a preset pressure. Some critical procedures are as follows.

(1) As deionized water would not cause the water quality disturbance to the seepage process, it was used to provide blank values for the study of water-rock interaction

(2) After samples were put in the rock sample loading and permeation system, bolts on both ends of the device were tightened. As confining pressure and axial pressure were applied simultaneously by a same degree, core samples would not be damaged and deformed due to the unbalance between confining pressure and axial pressure

(3) Check the stability of the equipment after the confining pressure system and the axial pressure system were fully applied. Parameters including real-time

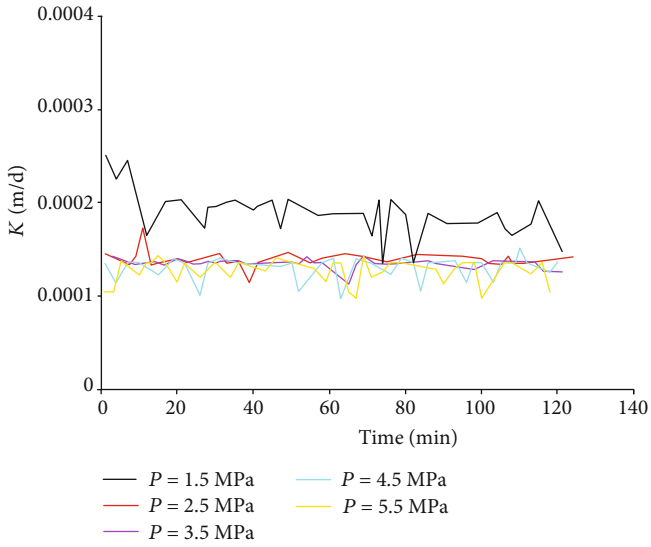

Figure 5: The variation curves of hydraulic conductivity of the preliminary seepage experiments.

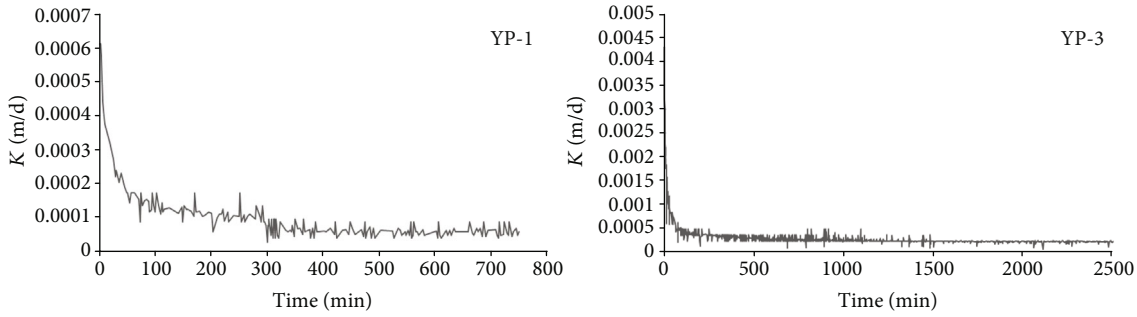

Figure 6: The hydraulic conductivity curve of YP-1 and YP-3.

confining pressure, axial pressure, time, injection pressure, and the volume of water flow were automatically recorded

(4) When the evolution characteristics of permeability was successfully recorded, the seepage process was prolonged to obtain enough aqueous solution (>250 ml). The aqueous solution that seeped through the samples was analyzed for its chemical composition. When experiments were over, saturated samples were weighed carefully. They were weighed again with an accuracy of 0.01 g after they have been dried off. Dry samples were saved for further analysis, including helium porosity, mercury intrusion, and SEM

(5) When the system stabilized, dynamic seepage experiments were initiated. The water injection was set at three different levels (0.5, 0.8, and 1 ml/min), each of which lasted ten minutes. Three different levels of injection were performed alternatively to create a hydrodynamic disturbance environment that enables materials within the pores to migrate. This dynamic process would last one hour. When the dynamic process was over, experiment parameters of the system were reset to the original value for measuring the hydraulic conductivity

4.2. Results. Due to the special mechanical characteristic and water-physical property of weakly cemented sandstone, some seepage experiments of rock samples cannot provide available permeability data. In this experiment, half of the rock samples provide the effective permeability parameters data, and there are only three rock samples with permeability mutation phenomenon. The variation curve of hydraulic conductivity of sandstone samples with time is given based on Equation (1), see Figure 6 and the S2-S5 in the Supplementary Material. According to the experiments, the seepage process of weakly cemented sandstones can be divided into the saturated seepage stage, the stable seepage stage, and the seepage mutation stage. This division conforms with the pattern of the hydraulic conductivity curves.

Each stage represents a different degree of water-rock interaction. As the real confined aquifer has always been saturated and without saturation process, the data of the first stage is of little use to our study. This paper mainly focused on the data of the latter two stages.

(1) The saturated stage. According to the results of XRD and SEM, quartz, potash feldspar, and albite constitute the framework of weakly cemented sandstones (Table 2). Kaolinite clay minerals serve as cements.

Table 2: X-ray diffraction quantitative analysis for whole sandstone.

Sample	Mineral content (%)			
	Quartz	Potash feldspar	Albite	Clay mineral (kaolinite; illite)
YP-2	38.1	21.0	24.4	14.1 (97; 3)
YP-3	61.8	14.4	7.2	15.6 (90; 10)
YP-6	51.0	9.8	20.1	16.8 (91; 9)
YP-9	44.2	21.5	16.1	16.8 (94; 6)
YP-21	53.2	17.8	17.0	15.5 (94; 6)

Table 3: The hydraulic conductivity in the saturated stage.

Sample	K (the initial) (m/d)	K (after two hours) (m/d)	The ratios
YP-1	0.00061	0.00006	0.0984
YP-3	0.0043	0.00042	0.0977
YP-6	0.0078	0.00080	0.1026
YP-14	0.0051	0.00056	0.1098
YP-21	0.0033	0.00041	0.1242
YP-22	0.0067	0.00059	0.0881
YP-23	0.0047	0.00046	0.0979

Table 4: The hydraulic conductivity of the stable stage.

Sample ID	K (m/d)	Sample ID	K (m/d)
YP-1	0.00006	YP-15	0.00007
YP-2	0.00004	YP-21	0.00024
YP-3	0.00023	YP-22	0.00023
YP-6	0.00040	YP-23	0.00027
YP-14	0.00012	YP-24-1	0.00005

Kaolinite occurs as multiple layers, sheets, and particles within or at the surface of the minerals, complicating the pore structures of weakly cemented sandstones (Figure 4). Kaolinite is liable to swell on contact with water, blocking up pore throats and channels of pore structures. As a result, the hydraulic conductivity of samples plummeted in the first two hours of the saturated phase. The hydraulic conductivity decreased to one tenth of the initial value (Table 3), accompanied by the occurrence of suspended matter in the aqueous solution. The suspended matter turned out to be kaolinite by testing.

(2) The stable stage. After the samples were saturated with water, pore structures and material distribution of the samples stabilized again, bringing the experiments into the stable phase. As shown in Figure 6, the hydraulic conductivity basically remains the same with a small variation. The specific data is given in Table 4.

(3) The seepage mutation stage. Hydrodynamic disturbance seepage experiments were performed on samples YP-1, YP-2, YP-3, YP-6, YP-14, YP-15, YP-21, YP-22, YP-23, and YP-24-1. The abrupt change of hydraulic conductivity occurred in the experiments of samples YP-2, YP-15, and YP-21, see Figure 7 and S6 in the supplementary materials.

The largest ratio of hydraulic conductivity before and after the abrupt change exceeded 10 (Table 5). At the same time, the flow of aqueous solution increased significantly, accompanied by the occurrence of large quantum of suspended matter, which is kaolinite. The continuous increase of hydraulic conductivity of weakly cemented sandstones under the condition of hydrodynamic disturbance is validated by laboratory experiments firstly, providing a basic experimental date for the further study on the evolution characteristic of the permeability.

5. Discussion

5.1. Variations in Micropore Structures. Based on the seepage experiments, the influence of water-rock interaction on the micropore structure is comprehensively integrated and analyzed by the result of hydrochemical tests, helium porosity, mercury intrusion experiments, and SEM. Correlations between pore parameters including porosity, the distribution of pore throats, and the mercury extrusion rate were identified. The coupling relationship between porosity, pore-throat distribution, mercury extrusion rate, and permeability can illustrate the influence of transformation in micropore structures on the permeability of weakly cemented sandstones.

5.1.1. Porosity. Porosity measurement is known as an efficient tool for investigating the micropore structures of rocks. The helium was injected into the samples by a helium porosimeter without structural damage and change; then, the porosity was tested. Results are given in Table 6. It should be noted that postexperiment porosity measurements were conducted on the saturated samples after they were dried off.

The porosity of all samples increased. The growth rate ranges from 1.82% to 11.38%, with an average rate of 4.16%. It is inferred that the migration or seepage of materials such as kaolinite within the pore is responsible for the increase of porosity. The increase of porosity has a positive effect on the seepage efficiency, improving the permeability of sandstones. As shown in Figure 8, the hydraulic conductivity increases as the porosity increases in most cases. Yet, no obvious linear correlation can be identified.

5.1.2. The Distribution of Pore Throats. Pores in sandstones are the main space for fluids, while the minimum pore throats serve as critical channels for the migration of that [22]. Fluids go through various pores and pore throats when flowing through the complicated pore structures of materials. We investigated the change of the distribution of pore throats by analyzing the average radius of pore throats and the ratio of throats to pores.

(1) The average radius of pore throats. The average pore-throat radius ($\bar{\delta}$) in rocks can be used to assess the connectivity of pores and the width of pore throats. The

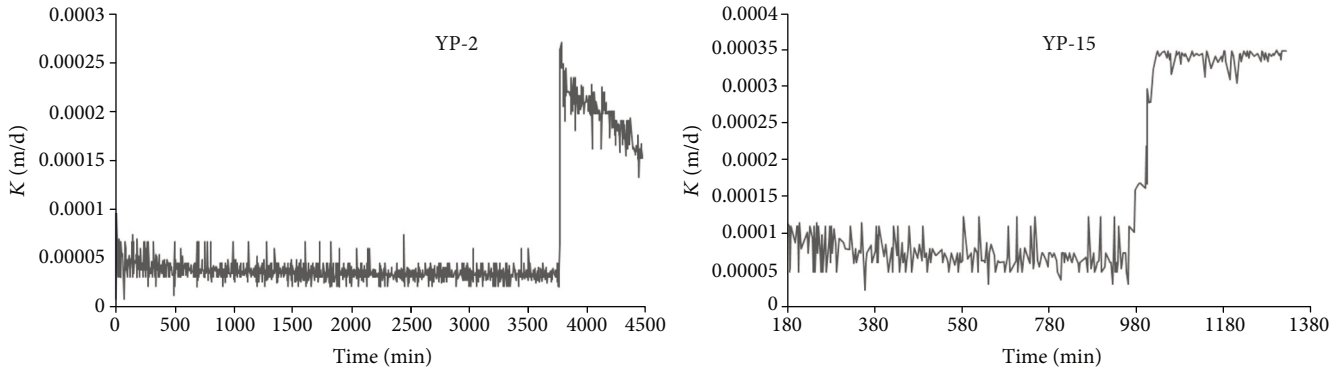

Figure 7: The hydraulic conductivity curves of YP-2 and YP-15.

Table 5: The hydraulic conductivity of samples YP-2, YP-15, and YP-21 before and after the change.

Sample	K (before) (m/d)	K (after) (m/d)	The ratio (%)
YP-2	0.00004	0.00027	6.75
YP-15	0.00007	0.00034	4.60
YP-21	0.00024	0.00240	10.0

Table 6: Porosity of the samples before and after the seepage experiments.

Sample	Preexperiment porosity	Postexperiment porosity	Growth rate
YP-1	27.33	30.44	11.38%
YP-2	31.05	32.25	3.86%
YP-3	32.80	33.52	2.20%
YP-6	31.55	32.30	2.38%
YP-8	26.21	27.16	3.62%
YP-9	25.47	26.16	2.71%
YP-14	27.02	27.96	3.48%
YP-15	29.14	29.67	1.82%
YP-16	30.70	31.77	3.49%
YP-21	34.45	35.69	3.60%
YP-22	32.84	34.34	4.57%
YP-23	32.23	33.35	3.48%
YP-24-1	28.37	29.93	5.50%

average pore-throat radius of samples before and after the seepage experiments was obtained by mercury intrusion experiments (Table 7).

The average pore-throat radius can signify the influence of water-rock interaction on pore throats. The average pore-throat radius of samples YP-2 and YP-21 increased due to water-rock interaction. That of samples YP-3 and YP-6 decreased, especially the decreasing trend of YP-6 was very obvious. Generally, the change of the average pore-throat radius is consistent with the trends of hydraulic conductivity. A linear correlation between the average pore-throat radius and the hydraulic conductivity was identified (Figure 9). The correlation coefficient is about 0.7349.

(2) The pore-throat ratio. The pore-throat ratio is the ratio of pore volume to throat volume in all pore throat intervals [23, 24]. The smaller the value, the better the seepage. This ratio of samples before and after the seepage experiments was obtained from the data of mercury intrusion experiments (Table 8). After the seepage experiments, the ratios of samples YP-2 and YP-21 decreased by 0.24 and 1.14, respectively. The ratios of samples YP-3 and YP-6 increased substantially after the seepage experiments. Influenced by the variation law of the pore-throat ratio, the hydraulic conductivity of the first two samples increases abruptly, and that of the latter two samples tend to be stable.

5.1.3. The Mercury Extrusion Rate. The mercury extrusion rate signifies the permeability and water yield property of sandstones [25]. The mercury extrusion rate of samples increased 1.54% to 8.67%, suggesting that the volume of pores within the weakly cemented sandstones expanded due to water-rock interaction. As shown in Figure 10, there is a poor positive correlation between the hydraulic conductivity and the mercury extrusion rate of the preexperiment samples and the postexperiment samples. It suggests that the mercury extrusion rate cannot be used to quantitatively determine the permeability of sandstones.

All in all, in the case of samples in which the abrupt change of hydraulic conductivity occurred, porosity, the mercury removal rate, and the average pore-throat radius increased after the seepage experiments. The pore-throat ratio decreased. In other samples, the average pore-throat radius tends to decrease, while the pore-throat ratio increased significantly. The jam of the seepage channels prevented the occurrence of the seepage mutation stage. The hydraulic conductivity increases as the porosity increases in most cases. Yet, no obvious correlation can be identified. There is a linear positive correlation between the hydraulic conductivity and the average pore-throat radius.

5.2. Construction of the Microseepage Model and Equation. The hydraulic conductivity of porous medium characterizes the flow resistance of the seepage process and

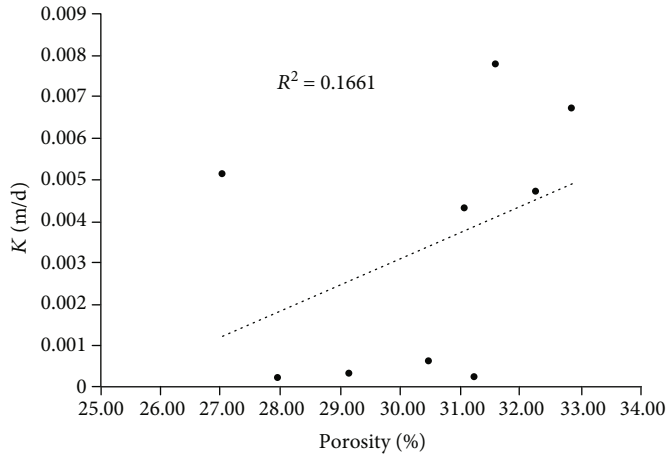

Figure 8: Correlation curves of the hydraulic conductivity and porosity.

Table 7: The average pore-throat radius of samples before and after the seepage experiments.

Sample	Preexperiment (μm)	Postexperiment (μm)
YP-2	0.105	0.129
YP-3	0.207	0.191
YP-6	0.450	0.224
YP-21	0.331	0.392

comprehensively reflects the movement form of fluid within the pores. The hydraulic conductivity is determined by not only the microscopic structural features such as porosity, the distribution of pore throats, and cementation but also the physical properties of fluids including the volumetric weight and viscous strength. The correlation between hydraulic conductivity (K) and specific permeability (k) can be described by the equation.

$$K = \frac{\rho g}{\mu} k. \tag{2}$$

As the seepage experiments were conducted at a constant indoor temperature of 30°C, a constant μ of 0.806 mpa·s was applied. Therefore, the specific permeability is linearly correlated to the hydraulic conductivity. In sum, the variation of specific permeability of weakly cemented sandstones conforms with that of the hydraulic conductivity. The transformation of microscopic structures of sandstones radically changes their intrinsic-specific permeability.

There are several common microscopic seepage models, including the straight capillary model, the parallel model, and the bifurcation model. On account of the high porosity of weakly cemented sandstones, the complicated pore structures of sandstones were simplified as straight capillary, see Figure 11. A mathematical model was established based on this capillary model. An equation was further deduced to describe the micropore structures and specific permeability of weakly cemented sandstones. The straight capillary model is a common linear seepage model which consists of parallel straight capillaries with the same diameter.

Several assumptions were proposed to establish the model.

(1) There is only one-dimensional flow of water in the straight capillaries

(2) The diameter of each capillary is the same, and their seepage characteristics are also consistent

(3) The straight capillaries are evenly and regularly distributed

Based on mechanical equations of seepage, the flow of single capillary can be written as

$$q_0 = \pi {r_0}^2 \bar{v} = -\frac{\pi {r_0}^4}{8\mu} \frac{d}{dl}(P + \rho g h). \tag{3}$$

For a horizontal single capillary, the flow of seepage can be written as

$$\frac{\Delta p}{dl} = -\frac{d}{dl}(P + \rho g h). \tag{4}$$

The total flow of water that went through a single capillary of the seepage model can be written as

$$Q = \frac{\pi}{8} \frac{\Delta p}{h} \frac{r^4}{\mu}. \tag{5}$$

Then, the radius of capillaries is replaced with the average pore-throat radius of weakly cemented sandstones; the total flow can be written as

$$Q = -\frac{\pi \bar{\delta}^4}{128\mu} \frac{dp}{dl}, \tag{6}$$

where dp/dl denotes the pressure gradient of capillaries in the direction of seepage.

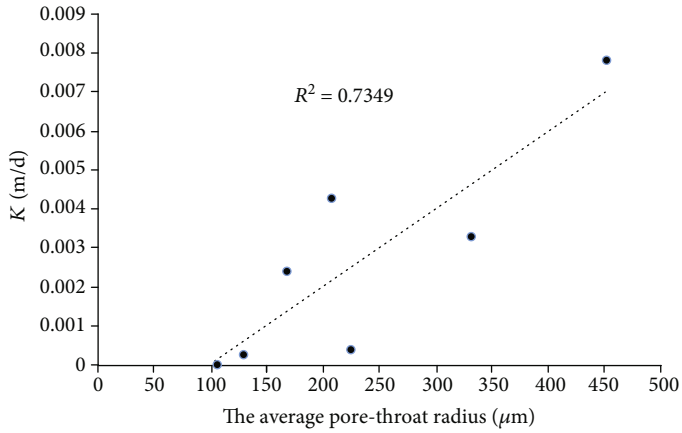

Figure 9: Correlation curves of the hydraulic conductivity and the average pore-throat radius

Table 8: The pore-throat ratio before and after the seepage experiments.

Sample	Preexperiment ratio	Postexperiment ratio
YP-2	1.5365	1.2923
YP-3	1.0714	20.4199
YP-6	2.5421	24.5813
YP-21	5.6653	4.2481

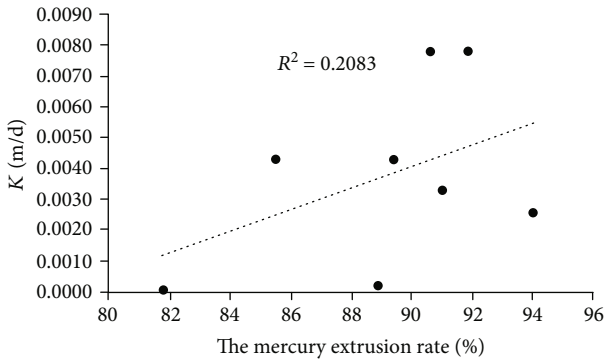

Figure 10: Correlation curves between the hydraulic conductivity and the mercury extrusion rate.

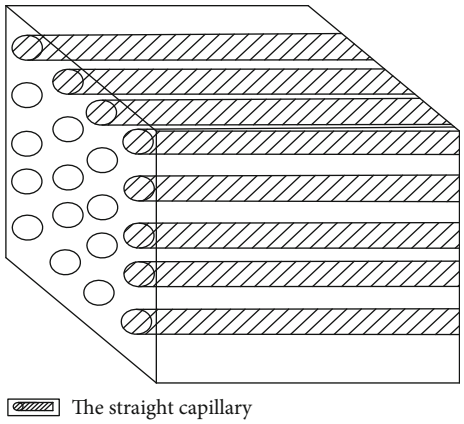

Figure 11: Schematic image of the straight capillary model.

We assumed that there were m capillaries per unit cross-section area; the flow per unit cross-section area can be written as

$$q = -\frac{m\pi\bar{\delta}^4}{128\mu}\frac{dp}{dl}. \tag{7}$$

Based on Darcy's law, q can be rewritten as

$$q = -\frac{k}{\mu}dpdl. \tag{8}$$

Equations (7) and (8) are merged as

$$k = -\frac{m\pi\bar{\delta}^4}{128\mu}. \tag{9}$$

As the pore volume of the direct capillary model is $m\pi\bar{\delta}^4/4$, its porosity can be written as

$$\phi = \frac{m\pi\bar{\delta}^4}{4}, \tag{10}$$

when m is canceled in Equations (9) and (10), the following equation is gotten

$$k = \frac{\phi\bar{\delta}^2}{32}. \tag{11}$$

According to Equation (11), the specific permeability of weakly cemented sandstones is directly proportional to porosity and the square of the average pore-throat radius. This correlation from the theoretical equation is consistent with the results of seepage experiments.

5.3. Evaluation of the Theoretical Equation. As the specific permeability is closely associated with their micropore structures, any small change in the microstructures would lead to the variation of permeability. To determine the accuracy and practicability of the theoretical equation for specific

Table 9: Theoretical and actual specific permeability of samples in the stable stage of experiments.

Sample	$\bar{\delta}$ (μm)	Porosity	Theoretical specific permeability (mD)	Actual specific permeability (mD)
YP-1	0.094	0.3044	0.0852	0.0578
YP-2	0.105	0.2733	0.0954	0.0386
YP-3	0.191	0.3280	0.3872	0.2217
YP-6	0.224	0.3155	0.5132	0.3856
YP-14	0.146	0.2796	0.1887	0.1157
YP-22	0.181	0.3434	0.3562	0.2217
YP-23	0.195	0.3335	0.4015	0.2603
YP-24-1	0.088	0.2993	0.0734	0.0482

Table 10: Theoretical and actual specific permeability of samples in the seepage mutation stage.

Sample	$\bar{\delta}$ (μm)	Porosity	Theoretical specific permeability (mD)	Actual specific permeability (mD)
YP-2	0.129	0.3044	0.1604	0.2603
YP-15	0.153	0.2967	0.2199	0.3277
YP-21	0.392	0.3352	1.7365	2.3135

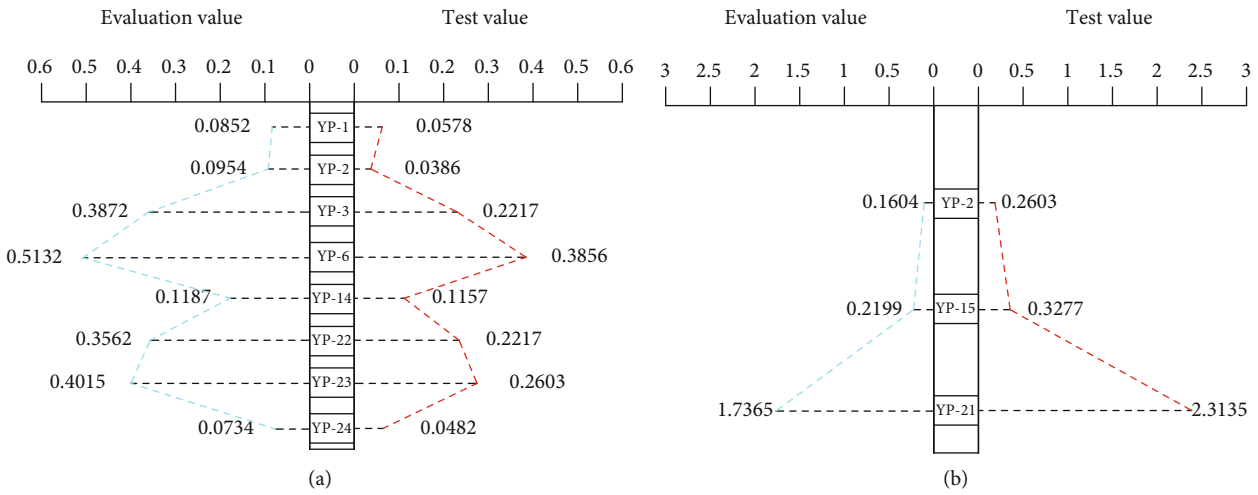

Figure 12: Comparative chart of theoretical and actual specific permeability.

permeability, the theoretical values obtained from the equation were compared with actual values in the latter two stages of the experiments (Tables 9 and 10). Then, we refined the equation based on Darcy's law.

As the comparative chart of theoretical and actual specific permeability shown in Figure 12, the variation trend of theoretical and actual values is approximately the same. It suggests that theoretical specific permeability can reflect the real specific permeability.

According to the statistic, the ratio of theoretical value and actual value varies from 1.33 to 1.62, with an average of 1.5 in the stable seepage stage. The interaction between kaolinite and water dominates and was the main contributing factor to kaolinite clay swelling. Water molecules were preferentially adsorbed onto oxygen and hydrogen atoms in kaolinite [26], see Figure 11. Taking this into consideration, the porosity and average pore-throat radius that were used in the theoretical equation are larger than actual values, resulting in a larger theoretical specific permeability. To diminish the deviation, the equation for specific permeability in the stable seepage stage was modified as

$$k = \frac{1}{\beta}\frac{\phi\bar{\delta}^2}{32}. \tag{12}$$

According to the statistic, the ratio of actual value and theoretical value varies from 1.33 to 1.62, with an average of 1.5 in the seepage mutation stage. The seepage channel expanded suddenly affected by a hydrodynamic disturbance

Table 11: Tests for significant differences between corrected theoretical values and actual values.

Difference source	SS	df	MS	F	P value	F crit
Original equation	0.035269	1	0.035269	1.569136	0.230853	8.861593
Correction equations	0.000365	1	0.000365	0.01137	0.916594	8.861593

environment. The flow increased sharply, resulting in a larger actual specific permeability. The equation for specific permeability in seepage mutation stage is modified as

$$k = \beta \frac{\phi \bar{\delta}^2}{32}, \tag{13}$$

where β denotes the correction coefficient.

To verify the effectivity of correction equations, tests for significant differences between corrected theoretical values and actual values were performed. As shown in Table 11, $F_C < F_O < F$ crit (0.01), indicating that the calculation and prediction level of permeability improved.

The transformation of microstructures of weakly cemented sandstones during the seepage process radically changes the specific permeability, posing great challenges to water control of coal mines in western China. The theoretical equation of specific permeability of weakly cemented sandstones can be used to provide valuable information for the exploitation and preservation of water in the study area.

6. Conclusion

In this experiment study, the permeability characteristic of weakly cemented sandstone was investigated. The main conclusions are drawn as follows:

(1) The seepage process of weakly cemented sandstones can be divided into the saturated seepage stage, the stable seepage stage, and the seepage mutation stage. The abrupt change of permeability in weakly cemented sandstones occurred under a hydrodynamic disturbance condition

(2) The pore-throat ratio can be used as a critical indicator for the abrupt change of permeability in weakly cemented sandstones

(3) A seepage model of straight capillary for micropore structures of weakly cemented sandstones was established, and the theoretical equation to calculate specific permeability of weakly cemented sandstones in the latter two stages of the seepage experiments was also proposed. It can be used to quantitatively evaluate the relation between specific permeability and micropore structures of weakly cemented sandstones

Symbols

Q_i: Volume of liquid during the ith time interval (m^3)
L: Length of core samples (m)
Δh: Variation of water pressure (m)
A: Cross-section area (m^2)
t: The ith time interval (d)
K: Hydraulic conductivity (m/d)
k: Specific permeability (mD)
μ: Dynamic viscosity (mpa·s)
$\varnothing$: Porosity
$\bar{\delta}$: The average pore-throat radius (μm)
β: Correction coefficient.

Data Availability

The data that support the findings of this study are provided in the supplementary material.

Conflicts of Interest

No conflict of interest was declared.

Acknowledgments

The authors acknowledge the financial support from the National Basic Research Program of China (973) Funded Project (Grant No. 2013CB227900) and the National Key R&D Program of China (Grant No. 2017YFC0804101). The authors also acknowledge the Joint Funds of the National Natural Science Foundation of China (U1710258) and the National Natural Science Foundation of China (Grant Nos. 51574172, and 41902180).

Supplementary Materials

The supplementary material includes the technology methodology of this study and the hydraulic conductivity curves. *(Supplementary Materials)*

References

[1] Q. Ma, Z. H. Zhao, X. J. Gao, S. J. Chen, and Y. L. Tan, "Numerical survey on the destabilization mechanism of weakly cemented soft rock roadway considering interlayer effect," *Geotechnical and Geological Engineering*, vol. 37, no. 1, pp. 95–105, 2019.

[2] Z. K. Wang, W. P. Li, Q. Wang, S. Liu, Y. Hu, and K. Fan, "Relationships between the petrographic, physical and mechanical characteristics of sedimentary rocks in Jurassic weakly cemented strata," *Environment and Earth Science*, vol. 78, no. 5, pp. 1–13, 2019.

[3] L. B. Brouwers, "A closer look: petrographic analysis of extremely weak sandstone/cemented sand of the Ghayathi Formation, Dubai, UAE," in *Latest Advancements in Underground Structures and Geological Engineering. GeoMEast 2019. Sustainable Civil Infrastructures*, A. Bezvijen, W. Wittke, H. Poulos, and H. Shehata, Eds., Springer, Cham, 2020.

[4] Q. Liu, Y. Sun, Z. Xu, X. Wang, C. Zhang, and M. Yao, "Pore media characteristics of Jurassic weak cemented sandstone and its significance for water-preserved mining," *Journal of China Coal Society*, vol. 44, no. 3, pp. 857–864, 2019.

[5] G. R. Krishnan, X. L. Zhao, M. Zaman, and J. C. Roegiers, "Fracture toughness of a soft sandstone," *International Journal of Rock Mechanics and Mining Sciences*, vol. 35, no. 6, pp. 695–710, 1998.

[6] X. Q. Zhang, T. X. Hang, J. Liu, and C. H. Yang, "Controls on the composition and distribution of the clay minerals from the Jurassic sandstone reservoirs in the Turpan-Hami Basin, Xinjiang," *Sedimentary Geology and Tethyan Geology*, vol. 21, no. 4, pp. 66–69, 2001, (In Chinese).

[7] S. You, H. G. Ji, T. Wang, and Z. Song, "Thermal and mechanical coupling effects on permeability of weakly cemented sandstone," *Emerging Materials Research*, vol. 7, no. 2, pp. 100–108, 2018.

[8] Q. Yu, Z. Dai, Z. Zhang, M. R. Soltanian, and S. Yin, "Estimation of sandstone permeability with SEM images based on fractal theory," *Transport in Porous Media*, vol. 126, no. 3, pp. 701–712, 2019.

[9] B. Li, Q. C. Ling, Z. Y. Bao, and S. Y. Xie, "Application of digital image processing to determination of petrophysical property," *Xinjiang Petroleum Geology*, vol. 29, no. 2, pp. 253–255, 2008.

[10] S. Bloch and K. P. Helmold, "Approaches to predicting reservoir quality in sandstones," *AAPG Bulletin*, vol. 79, no. 1, pp. 97–115, 1995.

[11] A. M. S. Lala, "A new universal permeability model derived from mercury capillary pressure data," *Arabian Journal of Geosciences*, vol. 8, no. 5, pp. 2567–2575, 2015.

[12] M. M. Herron, "Estimating the intrinsic permeability of clastic sediments from geochemical data," *SPWLA 28th Annual Logging Symposium*, 1987, London, England, June-July 1987, 1987Society of Petro physicists and Well-Log Analysts.

[13] J. Kozeny, "Ueber kapillare leitung des wassers im boden," *Sitzungsberichte Wiener Akademie*, vol. 136, no. 2a, pp. 271–306, 1927.

[14] P. C. Carman, "Fluid flow through granular beds," *Chemical Engineering Research and Design*, vol. 75, no. 1, pp. S32–S48, 1937.

[15] A. Timur, "An investigation of permeability, porosity, and residual water saturation relationship for sandstone reservoirs," *The Log Analyst*, vol. 9, no. 4, pp. 8–17, 1968.

[16] A. Timur, "Producible porosity and permeability of sandstones investigated through nuclear magnetic resonance principles," *The Log Analyst*, vol. 10, no. 1, pp. 3–11, 1968.

[17] W. C. Krumbein and G. D. Monk, "Permeability as a function of the size parameters of unconsolidated sand," *Transactions of the AIME*, vol. 151, no. 1, pp. 153–163, 2013.

[18] H. G. Ji, H. Jiang, Z. Y. Song et al., "Analysis on the microstructure evolution and fracture morphology during the softening process of weakly cemented sandstone," *Journal of China Coal Society*, vol. 43, no. 4, pp. 993–999, 2018.

[19] B. Ataie-Ashtiani, R. E. Volker, and D. A. Lockington, "Numerical and experimental study of seepage in unconfined aquifers with a periodic boundary condition," *Journal of Hydrology*, vol. 222, no. 1-4, pp. 165–184, 1999.

[20] G. W. Su, J. T. Geller, K. Pruess, and F. Wen, "Experimental studies of water seepage and intermittent flow in unsaturated, rough-walled fractures," *Water Resources Research*, vol. 35, no. 4, pp. 1019–1037, 1999.

[21] R. T. Armstrong, J. E. McClure, M. A. Berrill, M. Rücker, S. Schlüter, and S. Berg, "Beyond Darcy's law: the role of phase topology and ganglion dynamics for two-fluid flow," *Physical Review E*, vol. 94, no. 4, article 043113, 2016.

[22] J. Bloomfield, D. Gooddy, M. Bright, and P. Williams, "Pore-throat size distributions in Permo-Triassic sandstones from the United Kingdom and some implications for contaminant hydrogeology," *Hydrogeology Journal*, vol. 9, no. 3, pp. 219–230, 2001.

[23] J. Fu, "Flow characteristics of viscoelastic polymer solution in expansion micro-pores of different pore-throat ratio," *Applied Mechanics and Materials*, vol. 268-270, no. 1, pp. 1119–1122, 2012.

[24] P. Li, M. Zheng, H. Bi, S. Wu, and X. Wang, "Pore throat structure and fractal characteristics of tight oil sandstone: a case study in the Ordos basin, China," *Journal of Petroleum Science and Engineering*, vol. 149, pp. 665–674, 2017.

[25] I. Chatzis and F. A. L. Dullien, "Mercury porosimetry curves of sandstones. Mechanisms of mercury penetration and withdrawal," *Powder Technology*, vol. 29, no. 1, pp. 117–125, 1981.

[26] B. Zhang, J. T. Kang, and T. H. Kang, "Effect of water on methane adsorption on the kaolinite (0 0 1) surface based on molecular simulations," *Applied Surface Science*, vol. 439, pp. 792–800, 2018.